Lab on a Chip

PAPER

View Article Online
View Journal | View Issue

Cite this: *Lab Chip*, 2018, **18**, 1914

Ultrahigh-throughput droplet microfluidic device for single-cell miRNA detection with isothermal amplification†

Song Guo, [a] Weikang Nicholas Lin,[ab] Yuwei Hu,[a] Guoyun Sun,[ab] Dinh-Tuan Phan [a] and Chia-Hung Chen *[abc]

Analysis of microRNA (miRNA), a pivotal primary regulator of fundamental cellular processes, at the single-cell level is essential to elucidate regulated gene expression precisely. Most single-cell gene sequencing methods use the polymerase chain reaction (PCR) to increase the concentration of the target gene for detection, thus requiring a barcoding process for cell identification and creating a challenge for real-time, large-scale screening of sequences in cells to rapidly profile physiological samples. In this study, a rapid, PCR-free, single-cell miRNA assay is developed from a continuous-flow microfluidic process employing a DNA hybridization chain reaction to amplify the target miRNA signal. Individual cells are encapsulated with DNA amplifiers in water-in-oil droplets and then lysed. The released target miRNA interacts with the DNA amplifiers to trigger hybridization reactions, producing fluorescence signals. Afterward, the target sequences are recycled to trigger a cyclic cascade reaction and significantly amplify the fluorescence signals without using PCR thermal cycling. Multiple DNA amplifiers with distinct fluorescence signals can be encapsulated simultaneously in a droplet to measure multiple miRNAs from a single cell simultaneously. Moreover, this process converts the lab bench PCR assay to a real-time droplet assay with the post-reaction fluorescence signal as a readout to allow flow cytometry-like continuous-flow measurement of sequences in a single cell with an ultrahigh throughput (300–500 cells per minute) for rapid biomedical identification.

Received 14th April 2018,
Accepted 30th May 2018

DOI: 10.1039/c8lc00390d

rsc.li/loc

Introduction

MicroRNAs (miRNAs), an important group of noncoding RNAs with lengths ranging from 18–25 nucleotides, regulate the physiological expression levels in individual cells.[1,2] Through molecular complementarity, miRNAs can regulate the cellular expression of mRNA targets, resulting in mRNA degradation or translation.[2] The ultimate consequences of miRNA regulation in a cell are alterations in protein expression and cellular homeostasis processes, such as cell differentiation, proliferation and death.[3,4] Thus, sensitive measurement of a miRNA in single cells is essential to analyze its biological mechanism and functionality.[5]

Polymerase chain reaction (PCR) is a promising amplification strategy to increase the levels of target DNA/RNA sequences for measurements with high sensitivity, but this method has limited capability to directly detect miRNAs due to the short length of miRNA molecules, which must act as a PCR template. To address this technical challenge, reverse transcription quantitative PCR (RT-qPCR), microarray, northern blot and next-generation sequencing (NGS) were developed to detect miRNAs to evaluate the roles of miRNAs in regulating gene expression in cells for clinical measurements. RT-qPCR was investigated as a method to transform a short miRNA into a long chain by either adding poly(A) tails or using a stem-loop probe. RT-qPCR is a promising method to measure miRNA with high specificity and absolute quantification but requires the design of complicated probes.[6] Northern blot, which involves the use of electrophoresis to separate RNA samples by size and detection with a hybridization probe complementary to a part of or the entire target sequence, suffers from low sensitivity.[7] A hybridization-based microarray with a gene probe was investigated to capture fluorescently tagged miRNAs for high-throughput detection, but the challenge of limited sensitivity remained.[8] NGS was developed as a powerful tool to measure miRNA with ultrahigh sensitivity for a wide range of quantitative biological and clinical applications.[9]

[a] *Department of Biomedical Engineering, National University of Singapore, 21 Lower Kent Ridge Road, 119077 Singapore. E-mail: biecch@nus.edu.sg*
[b] *Biomedical Institute for Global Health Research and Technology (BIGHEART), National University of Singapore, 21 Lower Kent Ridge Road, 119077 Singapore*
[c] *Singapore Institute of Neurotechnology (SINAPSE), National University of Singapore, 21 Lower Kent Ridge Road, 119077 Singapore*

† Electronic supplementary information (ESI) available. See DOI: 10.1039/c8lc00390d

Recently, microfluidic platforms have been developed to isolate single cells to determine their miRNA expression levels *via* PCR.[10–12] For example, a microwell array with valves was employed to compartmentalize individual cells for single-cell sequencing with precise sequential control, but the throughput was limited to ~100 cells per experimental run. Because of the limited number of screened cells, the connections between the screening result and the biological sample profile were unclear.[13] Droplet-based microfluidics were investigated for a wide range of high-throughput single-cell measurements.[14,15] In 2015, D. A. Weitz *et al.* pioneered the utilization of the droplet single-cell RNA assay, which is now a commercial platform for single-cell assays, for biological sample profiling.[16] Since then, creative works in many laboratories have led to the development of various single-cell RNA/DNA/protein assays using droplet microfluidics, enabling applications in quantitative biology[17,18] and bacterial detection.[19,20] With effective droplet-based compartmentalization of single cells, individual cells were encapsulated within water-in-oil droplets for RNA sequencing.[21,22] After cell lysis in a droplet, RNA targets were released into the droplet and initiated the polymerization process involving reverse transcriptase. Through the incorporation of barcoding hydrogel beads in the droplets to label the RNA of a specific cell, rich single-cell RNA information could be obtained by PCR after the droplets break in a solution. With this technology, the throughput of single-cell RNA detection could approach 10^4 cells for biological sample profiling with statistical meaning.[23] This barcoding protocol was investigated to identify a stem cell profile,[23] bacterial activities in a solution[24] and a mutant cell profile.[25] Precise single-cell RNA analysis was demonstrated using an error-correcting code (ECC).[26] With further optimization, this technology was applied to identify multiple proteins from single cells, demonstrating the flexibility of this powerful analytical method well.[27] Despite their advantages, most sequence-based methods for single-cell miRNA analysis require a delicate process (such as barcoding/enzyme degradation steps) to perform PCR, complicating the assays. Moreover, developing ultrahigh-throughput assays for low-cost, rapid profiling of physiological samples for diagnosis remains a challenge.

Recently, isothermal amplification has emerged as a powerful method for quantifying nucleic acids and has been used to measure miRNA with high specificity and sensitivity without precisely controlled temperature cycling. In contrast to PCR methods, which rely on thermocycling to amplify the target sequence, isothermal amplification can rapidly amplify the target sequence with signal recognition at a constant temperature by simple operations.[28] Therefore, this method is especially useful for analyzing short-chain RNAs such as miRNAs and is well suited to be incorporated into a microfluidic device for automated operation.[29] A wide range of isothermal amplification techniques, such as rolling circle amplification (RCA),[30,31] exponential amplification reaction (EXPAR),[32] displacement amplification,[33–35] duplex-specific nuclease signal amplification (DSNSA),[36] and loop-mediated isothermal amplification (LAMP),[37–40] were developed before. For example, Sidore *et al.* reported digital droplet multiple displacement amplification (ddMDA) to increase the target DNA concentration in a solution, through droplet compartmentalization for high sensitivity measurement.[34] Giuffrida *et al.* investigated the isothermal amplification method to detect and amplify microRNA-210 in microdroplets.[35] DNA polymerase-I was introduced to polymerize deoxynucleotides, causing the target displacement and recycled target miRNA to enhance the signal. However, these methods involved a long incubation time (~16 hours) and amplification by sequentially uploading multiple primers or enzymes. The enzyme-free methods, hybridization chain reaction (HCR) and catalytic hairpin assembly (CHA), were investigated by Dirks,[41] Yin[42] and Li[43] to confer high amplification efficiency with simple operations. Yin[42] described the concept of DNA self-assembly, where the DNA hairpin structure was designed and demonstrated for a variety of dynamic functions. However, the challenge in high background reactivity remained. To address this, Li *et al.*[43] modified the hairpin DNA sequence to reduce the background reactivity in the absence of a target. These methods were further adapted for single-cell miRNA imaging.[44,45] Recently, fluorescence *in situ* hybridization (FISH) has been developed to bind a fluorescent probe to target miRNA based on isothermal hybridization.[46,47] By using this chemical method to increase cell membrane permeability,[48–50] DNA probes were uploaded to individual cells for miRNA measurement *via* flow cytometry.[51] However, complicated multiple chemical steps were required to modify cell membranes for DNA probe intake. Moreover, FISH required a time consuming cell culturing process before screening. Therefore, the challenge in real time biological sample profiling remained.

In this study, a novel droplet process for single-cell miRNA non-enzymatic isothermal amplification was investigated; this process enabled rapid large-scale single-cell miRNA detection in a continuous-flow manner. The integration of droplet microfluidics and miRNA isothermal amplification is synergetic. Single cells and reagents were effectively isolated *via* droplet encapsulation, and miRNA isothermal amplification could spontaneously occur within the droplets for rapid target miRNA analysis. To develop an automatic process for single miRNA isothermal amplification in a droplet, our autonomous sequence hybridization amplification included two main processes. The first was a target recognition and recycling procedure involving two hairpin DNAs, in which conformational changes could be initiated by binding to the target miRNA. The second was a signaling procedure, where the previously hybridized hairpins triggered the separation of the fluorophore and quencher pairs by hybridizing the fluorophore-modified sequence, resulting in amplified fluorescence. This process is illustrated in Fig. 1. In the first step, the single cells, cell lysis solution (Triton X-100) and miRNA amplifier reagents (hairpin 1 : hairpin 2 : fluorophore : quencher = 400 : 1600 : 600 : 720 nM) were encapsulated in individual droplets. Upon cell lysis, target miRNAs (miRNA-21)

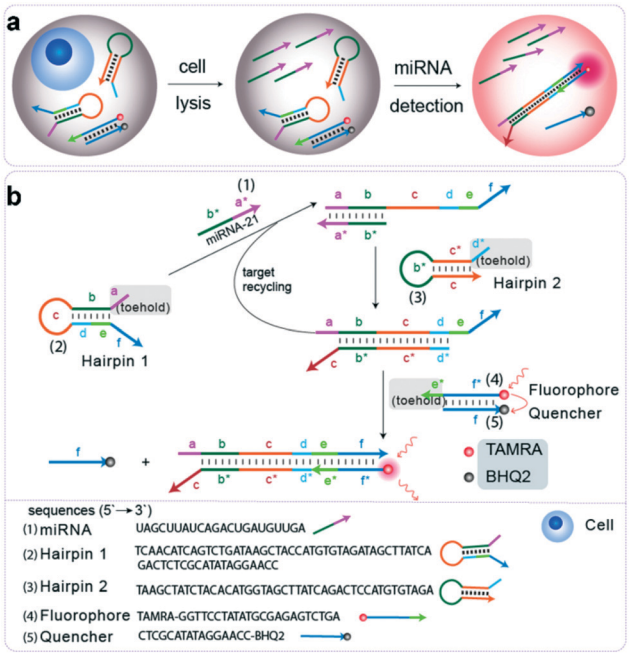

Fig. 1 (a) Illustration of the hairpin DNA isothermal amplifier for catalytic signal enhancement of the miRNA-21 expression in cells. After cell lysis, a HCR was initiated by the specific target mRNA-21 to repeatedly generate many H1–H2 complexes, which further separated the fluorophore (TAMRA) from the quencher (BHQ2) and enhanced the fluorescence inside the microdroplets. (b) Specific demonstration of the miRNA-induced autonomous DNA hybridization amplification.

were released and could mix with the reagents within the droplets, initiating a hybridization process. Afterward, the same miRNA would react again with another hairpin 2 to release more fluorophores, amplifying the fluorescence signals. Next, the droplets were flowed through an optical sensor customized for high-throughput detection in a continuous-flow manner (3–5k droplets per minute). MCF-7, MDA-MB-231 and MCF-10A cells were screened and showed distinct miRNA profiles, demonstrating the promising rapid identification of cells *via* the target miRNA (300–500 cells per minute). Because of the advantage of obtaining statistical information about single-cell miRNAs, the information about single-cell miRNAs and ensemble biological samples can be connected for precise, rapid profiling of physiological samples.

Results and discussion

Autonomous sequence hybridization amplification was performed by using miRNA-21, which is overexpressed in cancer cells, as a target. The sequences of miRNA-21 and the DNA amplifiers used in this study are illustrated in Fig. 1 (Supplementary-1†). In the presence of the target miRNA-21 (1), domain a* hybridizes with the toehold of hairpin H1 (2), which initiates the hybridization chain reaction (HCR) to form complex (1)/(2). Subsequently, the unblocked domain d of (2) hybridizes with toehold d* in hairpin H2 (3) to initiate the HCR, resulting in the formation of complex (2)/(3) due to the greater energetic favorability. Afterward, the target miRNA-21 (1) was recycled to open another hairpin H1 (2), repeating the reaction. Domain e in complex (2)/(3) hybridized with toehold e* in complex (4)/(5), forming complex (2)/(3)/(4) and single-stranded (5). The separation of the fluorophore (TAMRA) and the quencher (BHQ2) resulted in the enhanced fluorescence of the system, which indicated the presence of the target miRNA-21.

To determine the reaction progress of the HCR, two hairpin DNAs (H1 and H2) with or without the miRNA-21 target were separated on a polyacrylamide gel electrophoresis (PAGE) gel (Supplementary-2†), which showed distinct bands indicating a hybridization reaction (Fig. 2a). As shown in Fig. 2a, in the proof-of-concept assay, no interaction between H1 and H2 was observed in the absence of the miRNA-21 target (lane 3), which indicated that the cross-interaction between H1 and H2 is effectively blocked without the addition of the target DNA. The presence of miRNA-21 initiated the reaction to generate an H1–H2 duplex (lane 5), which was in accordance with the annealing of H1–H2 (lane 4). *In vitro* experiments were performed to characterize the HCR process (Supplementary-3†). The relation between the concentration ratio of H1 : H2 and the fluorescence intensity is shown in Fig. 2b. To ensure that all miRNA-21 targets were involved in the HCR for detection, the ratio of H1 : H2 was optimized at 1 : 4 in this study. To reach the HCR equilibrium within a short time, the concentration of hairpin H2 was optimized with a constant concentration ratio of H1 : H2 (1 : 4). As shown in Fig. 2c and S1, Supplementary-3,† with a high concentration of hairpin H1 (400 nM), the fluorescence intensity increased rapidly. To ensure all fluorophore DNAs were

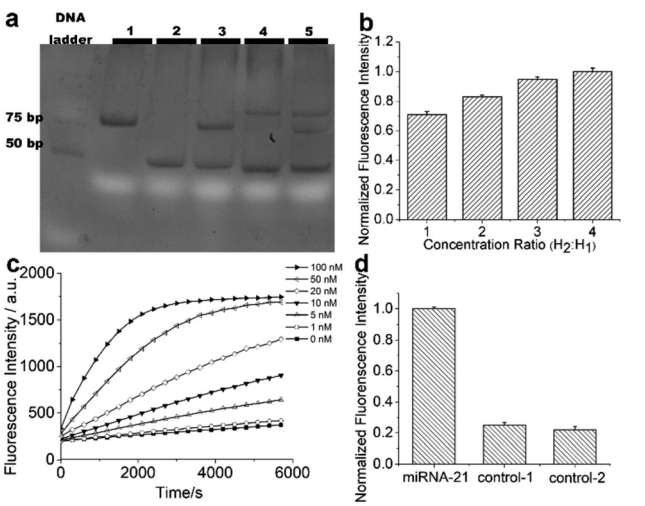

Fig. 2 (a) PAGE gel analysis: H1 (lane 1); H2 (lane 2); H1 and H2 mixtures (lane 3); annealing H1 and H2 (lane 4); H1 and H2 were reacted with the miRNA-21 target (lane 5). (b) Optimization of the concentration ratios of hairpin DNA (H2 : H1). (c) Fluorescence kinetics of the hairpin DNA reaction with various concentrations of the target DNA (0, 0.5, 1, 5, 10, 50, and 100 nM). The concentrations of H1, H2, fluorophore and quencher were 400, 1600, 600 and 720 nM, respectively. (d) Normalized fluorescence enhancement of the hairpin DNA reaction with the miRNA-21, control-1 and control-2 targets.

hybridized with quencher DNAs, which could reduce the background signal, the fluorophore : quencher ratio was 1 : 1.2. The optimized concentration of hairpin DNAs (hairpin 1 : hairpin 2 : fluorophore : quencher = 1600 : 400 : 600 : 720 nM) was applied throughout the subsequent experiments.

The sensitivity of the HCR was determined by a series of control experiments in which the miRNA concentration was from 1 nM to 100 nM. As expected, the fluorescence intensity increased with the target DNA concentration (Fig. 2c). At a high concentration of miRNA-21 (100 nM), the fluorescence intensity plateaued in 40 minutes. With the decrease in the miRNA concentration to 50 nM, the time to reach the plateau increased to 1 hour, and the maximum fluorescence intensity was decreased. When the miRNA concentration was further decreased, the time to reach the plateau continuously increased, and the maximum fluorescence intensity decreased. A negative control experiment was performed by mixing hairpin DNAs and mismatched miRNA and performing the HCR (Fig. 2d). In experiment 1, one type of mismatched miRNA (control-1) was used. Because of the mismatch with the toehold in hairpin H1, the hybridization reaction that would dramatically increase the fluorescence intensity was not triggered. Accordingly, a decrease in the fluorescence intensity change was clearly observed in control-1. The difference between miRNA-21 and control-1 was ~4.5-fold. In control experiment 2, two mismatched miRNAs (control-2) were employed. Similar to the control-1 experiment, the observed fluorescence increases were smaller than the fluorescence intensity increase obtained by mixing hairpin DNAs and miRNA-21. The difference between miRNA-21 and control-2 was ~5.1-fold. These results demonstrate the excellent selectivity of hairpin DNAs for identifying the target miRNA-21.

With the HCR characterization for miRNA-21 measurement, the HCR for single-cell miRNA-21 detection using droplet-based microfluidics was conducted (Supplementary-4†). Suspended cells were introduced into a microchannel from one inlet to mix with the hairpin DNA sequence & lysis buffer from another inlet to encapsulate single cells in water-in-oil droplets in Chip 1 (Fig. S2a, Supplementary 4†). A 1% Triton X solution has been added to the mixture solution to permeate cell membranes and cause *in situ* cell lysis in the droplets. To avoid the degradation of hairpin DNAs in the cell lysate, proteinase K (from *Tritirachium album*, Sigma, MO, USA) was added to the solution, which enabled rapid inactivation of the nucleases in the lysate. Both cell suspensions and hairpin DNA sequence & lysis buffer solutions were introduced into the co-flow channel using syringe pumps (Harvard, PHD2000). The oil flow rate was set at 6 μL min^{-1} while both aqueous flow rates were set at 1 μL min^{-1} to form ~30 pL droplets with a generation rate of ~1 kHz. Fluorocarbon oil HFE-7500 (3 M NovecTM, Singapore) with 0.5% surfactant (Pico-Surf 1, Dolomite Microfluidics) was used to generate stable, monodisperse 40 μm droplets *via* the flow-focusing droplet-generating microfluidic chip. During the formation of the water-in-oil droplets, two aqueous phases were mixed by the inertial flows generated within the droplets moving along the microchannel. After encapsulation, these droplets were collected in a chamber for fluorescence signal observation at room temperature (26 °C).

To determine the number of cells in the droplets, Hoechst 33342 (Life Technologies) was used to stain the cell nuclei. The cells used in the single-cell encapsulation experiments were first incubated with Hoechst 33342 (1 μg ml^{-1}) for 15 minutes to stain the live cells. Once the cell suspension was mixed with the lysis buffer, the permeability of the cell membrane increased with increases in the Triton (cell lysis reagent) concentration.[52] The miRNAs within the single cells were released into the droplet to mix with hairpin DNAs, leading to fluorescence signal increases. With the information about the miRNA activity (red channel, excitation/emission: 545/576 nm) and the cell number (blue channel, excitation/emission: 350/461 nm) in the droplets, single-cell miRNA could be obtained from the fluorescence signal increases (Fig. 3a). The encapsulation rate of cells was consistent with a Poisson distribution because of the random encapsulation of the cells in the droplets, with slight deviations resulting from clustering of the cells in experiments where an adherent cell line was used (Table S1, Supplementary-4†). After incubation for 20 minutes, the droplets containing the cells showed increased fluorescence signals (red channel) (Fig. 3b). The fluorescence signals reached a plateau in 40 minutes after encapsulation (Fig. S3 and S4, Supplementary-4†) when low concentrations of Triton were applied. The increase in fluorescence signals is shown in Fig. 3c and suggests that a single-cell miRNA-21 can be detected in 20 minutes *via* isothermal amplification in the droplets. Notably, a small fluorescence signal increase was observed in the droplets without cell encapsulation because of natural degradation of the hairpin sensors.

To develop an automatic system for high-throughput continuous-flow single-cell miRNA detection, we combined a droplet generator, incubation tube and optical sensor. After cell encapsulation, the droplets were flowed through a long

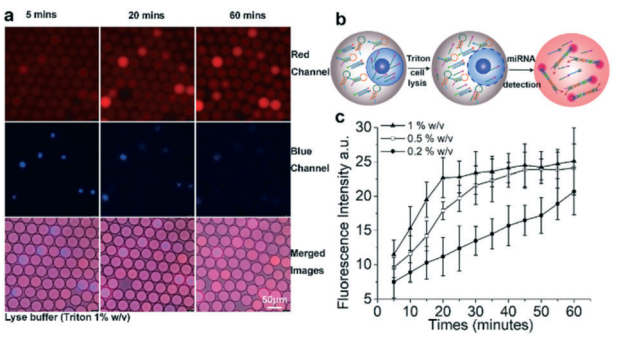

Fig. 3 Single-cell miRNA analysis in microdroplets. (a) An increase in the fluorescence intensity from the red channel was observed when the single cell was mixed with the lysis buffer in microdroplets. The concentration of Triton was 1.0% w/v. The merged images include bright-field images to show the droplets. (b) Schematic process of the cell lysis and miRNA detection at high Triton concentrations. (c) Fluorescence response for single-cell miRNA detection with various Triton concentrations (0.2, 0.5, and 1.0% w/v).

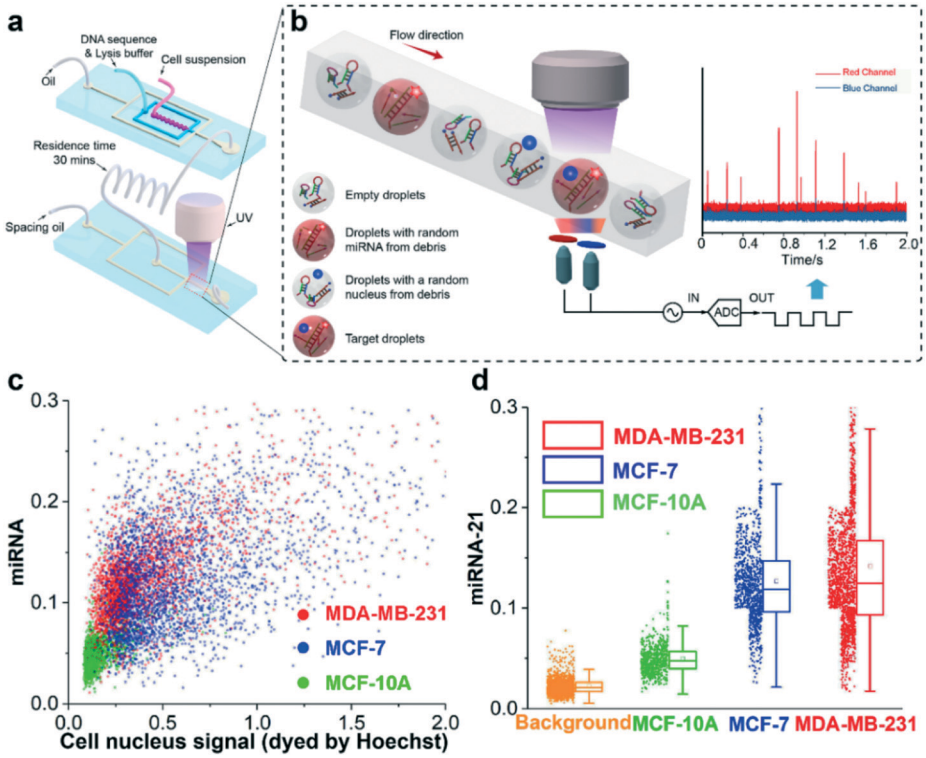

Fig. 4 (a) Scheme of the microfluidics-based online PMT analysis system. Single cells were encapsulated into droplets for miRNA-21 screening. (b) A multiband bandpass excitation filter and individual emission filters were used to allow efficient readout of multiple fluorescence signals into the PMT system. Fluorescence signals were detected as analog voltage outputs and subsequently converted to digital signals for computational calculation in real time. (c) Plots showing the distribution of MDA-MB-213, MCF-7 and MCF-10A in terms of signal intensity. Each dot represents a single cell. Green plot: MCF-10A, blue plot: MCF-7, and red plot: MDA-MB-231. (d) Box plot of the three cell lines and the background. Green box: MCF-10A, blue box: MCF-7, red box: MDA-MB-231, and yellow box: background.

polyethylene (PE) tube with an inner diameter of 0.38 mm (Scientific Commodities, USA). The length of the tube was optimized at 1.5 m, the residence time of which was 30 minutes for signal incubation at room temperature (26 °C). Afterward, the droplets were injected into Chip 2 (Fig. S2b, Supplementary-4†) with a photomultiplier (PMT) sensor for screening the post-reaction fluorescence signal (Fig. S5, Supplementary-5†). Spacing oil was used with a flow rate of 10 μl min^{-1} to ensure separation between droplets for PMT detection (Fig. 4a). The fluorescence signals were rapidly detected by two PMTs. The first PMT detected fluorescence signals with a wavelength of 453 nm to identify cell nuclei. The second PMT measured the fluorescence signals with a wavelength of 650 nm to identify miRNA-21. The optical fluorescence signals were converted to digital signals for fast real-time computational analysis (Fig. 4b). The throughput of this system was ~300 droplets per second. To avoid interference from random miRNA-21 and nuclei in the debris, the peak was observed simultaneously in two channels. The counting of single-cell miRNA activity was activated when two fluorescence signals were observed simultaneously in single droplets, providing a cell population distribution based on the RNA activity (Fig. 4c and S6, Supplementary-5†). *Via* comparison with the background fluorescence signal, the miRNA concentrations were quantified.

The miRNA-21 activities of two tumorigenic breast cell lines (MCF-7 and MDA-MB-231) and a non-tumorigenic breast cell line (MCF-10A) were determined by using this system. Both MDA-MB-231 and MCF-7 showed higher miRNA signal intensities than MCF-10A. This observation is consistent with previous studies using real-time PCR.[53,54] As metastatic breast cancer cells, both MCF-7 and MDA-MB-231 cells expressed high miRNA-21 levels.[55] As normal mammary epithelial cells, MCF-10A cells expressed a low level of miRNA-21. The single-cell miRNA-21 activities are quantified in Fig. 4d. The background was evaluated by measuring empty droplets. MCF-10A cells showed a low level of miRNA activity compared with the cancer cells (MCF-7 and MDA-MB-231). The difference in the miRNA expression level between MCF-7 and MDA-MB-231 cells was determined. As aggressive cancer cells, MDA-MB-231 cells (miRNA signal intensity was 0.142 a.u.) showed a slightly higher level of miRNA expression than MCF-7 cells (miRNA signal intensity was 0.127 a.u.). The difference in the miRNA expression level between MCF-7 and MDA-MB-231 cells was observed.

Conclusions

In summary, an integrated droplet microfluidic system for PCR-free single-cell miRNA screening with ultrahigh efficiency was developed. With a non-enzymatic hybridization

chain reaction (HCR) of specifically designed hairpin DNA sequences, the novel enzyme-free isothermal amplification of the target miRNA was spontaneously triggered to significantly amplify the fluorescence signals within 20 minutes in the droplets with single-cell lysis, enabling high-specificity measurements. Incorporating a customized photomultiplier (PMT) detector enabled the continuous-flow droplet screening of single-cell miRNA with a throughout of 300–500 cells per minute for the profiling of large-scale physiological samples. Single cells were dissociated from physiological samples and encapsulated into droplets for miRNA measurement. Excitation light passed through a bandpass filter to stimulate the red fluorescence produced by the HCR in the droplets to allow miRNA measurements using a PMT sensor. Three different samples, MCF-7 and MDA-MB-231 breast cancer cells and MCF-10A healthy breast cells, were screened by using this system. The cancer cells (MCF-7 and MDA-MB-231) showing high miRNA expression levels were clearly distinguished from the healthy cells (MCF-10A). Moreover, the aggressive cancer cells (MDA-MB-231) showed a higher miRNA expression level than the less aggressive cancer cells (MCF-7) in statistical analysis, as expected. The capability of using this system to rapidly profile a population distribution according to a single-cell target miRNA allows the elucidation of physiological sample states for rapid, precise biomedical analysis.

Author contributions

Song Guo, Yuwei Hu and Chia-Hung Chen designed the research; Song Guo performed the *in vitro* research; Song Guo, Weikang Nicholas Lin and Guoyun Sun performed the *in vivo* experiment. Song Guo, Guoyun Sun and Dinh-Tuan Phan analysed the data and draw the scheme pictures; Song Guo and Chia-Hung Chen wrote the paper.

Conflicts of interest

There are no conflicts to declare.

Acknowledgements

The authors gratefully acknowledge the financial support provided by the NMRC Industry Alignment Fund Category 1 (R-397-000-230-511), NRF BDTA (R-397-000-221-592), NRF EIRP (R-397-000-252-592), NRF CRP (R-397-000-276-281), MOE Tier-1 (R-397-000-213-112; R-397-000-248-112), and MOE Tier-2 (R-397-000-271-112, R-397-000-253-112) and the facilities provided by the Biomedical Institute for Global Health Research & Technology (BIGHEART). The human breast cell line MCF-10A and cancer cell lines MCF-7 and MDA-MB-231 were obtained from the American Type Culture Collection (ATCC) and cultured for single cell experiments.

Notes and references

1 C. C. Pritchard, H. H. Cheng and M. Tewari, *Nat. Rev. Genet.*, 2012, **13**, 358.
2 R. M. Graybill and R. C. Bailey, *Anal. Chem.*, 2016, **88**, 431.
3 D. P. Bartel, *Cell*, 2004, **116**, 281.
4 A. Lujambio and S. W. Lowe, *Nature*, 2012, **482**, 347.
5 C. Földy, S. Darmanis, J. Aoto, R. C. Malenka, S. R. Quake and T. C. Südhof, *Proc. Natl. Acad. Sci. U. S. A.*, 2016, **113**, E5222.
6 E. M. Kroh, R. K. Parkin, P. S. Mitchell and M. Tewari, *Methods*, 2010, **50**, 298.
7 A. Válóczi, C. Hornyik, N. Varga, J. Burgyán, S. Kauppinen and Z. Havelda, *Nucleic Acids Res.*, 2004, **32**, e175.
8 S. Pradervand, J. Weber, F. Lemoine, F. Consales, A. Paillusson, M. Dupasquier, J. Thomas, H. Richter, H. Kaessmann, E. Beaudoing, O. Hagenbüchle and K. Harshman, *BioTechniques*, 2010, **48**, 219.
9 M. L. Metzker, *Nat. Rev. Genet.*, 2010, **11**, 31.
10 F. Porichis, M. G. Hart, M. Griesbeck, H. L. Everett, M. Hassan, A. E. Baxter, M. Lindqvist, S. M. Miller, D. Z. Soghoian, D. G. Kavanagh, S. Reynolds, B. Norris, S. K. Mordecai, Q. Nguyen, C. F. Lai and D. E. Kaufmann, *Nat. Commun.*, 2014, **5**, 5641.
11 V. Sanchez-Freire, A. D. Ebert, T. Kalisky, S. R. Quake and J. C. Wu, *Nat. Protoc.*, 2012, **7**, 829.
12 S. C. Kim, I. C. Clark, P. Shahi and A. R. Abate, *Anal. Chem.*, 2018, **90**, 1273.
13 R. Tewhey, J. B. Warner, M. Nakano, B. Libby, M. Medkova, P. H. David, S. K. Kotsopoulos, M. L. Samuels, J. B. Hutchison, J. W. Larson, E. J. Topol, M. P. Weiner, O. Harismendy, J. Olson, D. R. Link and K. A. Frazer, *Nat. Biotechnol.*, 2009, **27**, 1025.
14 J. S. Marcus, W. F. Anderson and S. R. Quake, *Anal. Chem.*, 2006, **78**, 3084.
15 P. Kumaresan, C. J. Yang, S. A. Cronier, R. G. Blazej and R. A. Mathies, *Anal. Chem.*, 2008, **80**, 3522.
16 E. Z. Macosko, A. Basu, R. Satija, J. Nemesh, K. Shekhar, M. Goldman, I. Tirosh, A. R. Bialas, N. Kamitaki, E. M. Martersteck, J. J. Trombetta, D. A. Weitz, J. R. Sanes, A. K. Shale, A. Regev and S. A. McCarroll, *Cell*, 2015, **161**, 1202.
17 N. Habib, I. Avraham-Davidi, A. Basu, T. Burks, K. Shekhar, M. Hofree, S. R. Choudhury, F. Aguet, E. Gelfand, K. Ardlie, D. A. Weitz, O. Rozenblatt-Rosen, F. Zhang and A. Regev, *Nat. Methods*, 2017, **14**, 955.
18 F. Lan, B. Demaree, N. Ahmed and A. R. Abate, *Nat. Biotechnol.*, 2017, **35**, 640.
19 A. Rotem, O. Ram, N. Shoresh, R. A. Sperling, A. Goren, D. A. Weitz and B. E. Bernstein, *Nat. Biotechnol.*, 2015, **33**, 1165.
20 A. E. Saliba, S. C. Santos and J. Vogel, *Curr. Opin. Microbiol.*, 2017, **35**, 78.
21 P. Mair, F. Gielen and F. Hollfelder, *Curr. Opin. Chem. Biol.*, 2017, **37**, 137.
22 Y. S. Fu, H. Chen, L. Liu and Y. Y. Huang, *Anal. Chem.*, 2016, **88**, 10795.
23 H. S. Moon, K. Je, J. W. Min, D. Park, K. Y. Han, S. H. Shin, W. Y. Park, C. E. Yoo and S. H. Kim, *Lab Chip*, 2018, **18**, 775.
24 A. M. Klein, L. Mazutis, I. Akartuna, N. Tallapragada, A. Veres, V. Li, L. Peshkin, D. A. Weitz and M. W. Kirschner, *Cell*, 2015, **161**, 1187.

25 F. Lan, J. R. Haliburton, A. Yuan and Adam R. Abate, *Nat. Commun.*, 2016, **7**, 11784.
26 K. Eyer, R. C. L. Doineau, C. E. Castrillon, L. Briseño-Roa, V. Menrath, G. Mottet, P. England, A. Godina, E. Brient-Litzler, C. Nizak, A. Jensen, A. D. Griffiths, J. Bibette, P. Bruhns and J. Baudry, *Nat. Biotechnol.*, 2017, **35**, 977.
27 Z. T. Chen, W. X. Zhou, S. Qiao, L. Kang, H. F. Duan, X. S. Xie and Y. Y. Huang, *Nat. Biotechnol.*, 2017, **35**, 1170.
28 J. Abatemarco, M. F. Sarhan, J. M. Wagner, J.-L. Lin, L. Liu, W. Hassouneh, S.-F. Yuan, H. S. Alper and A. R. Abate, *Nat. Commun.*, 2017, **8**, 332.
29 Y. X. Zhao, F. Chen, Q. Li, L. H. Wang and C. H. Fan, *Chem. Rev.*, 2015, **115**, 12491.
30 R. J. Deng, K. X. Zhang and J. H. Li, *Acc. Chem. Res.*, 2017, **50**, 1059.
31 P. M. Lizardi, X. Huang, Z. Zhu, P. Bray-Ward, D. C. Thomas and D. C. Ward, *Nat. Genet.*, 1998, **19**, 225.
32 A. Cao and C. Y. Zhang, *Anal. Chem.*, 2012, **84**, 6199.
33 H. Jia, Z. Li, C. Liu and Y. Cheng, *Angew. Chem., Int. Ed.*, 2010, **49**, 5498.
34 A. M. Sidore, F. Lan, S. W. Lim and A. R. Abate, *Nucleic Acids Res.*, 2015, **44**, e66.
35 M. C. Giuffrida, L. M. Zanoli, R. D'Agata, A. Finotti, R. Gambari and G. Spoto, *Anal. Bioanal. Chem.*, 2015, **407**, 1533.
36 C. Shi, Q. Liu, C. Ma and W. Zhong, *Anal. Chem.*, 2014, **86**, 336.
37 B. C. Yin, Y. Q. Liu and B. C. Ye, *J. Am. Chem. Soc.*, 2012, **134**, 5064.
38 T. D. Rane, L. Chen, H. C. Zec and T. H. Wang, *Lab Chip*, 2015, **15**, 776.
39 N. Tomita, Y. Mori, H. Kanda and T. Notomi, *Nat. Protoc.*, 2008, **3**, 877.
40 N. G. Schoepp, T. S. Schlappi, M. S. Curtis, S. S. Butkovich, S. Miller, R. M. Humphries and R. F. Ismagilov, *Sci. Transl. Med.*, 2017, **9**, eaal 3693.
41 R. M. Dirks and N. A. Pierce, *Proc. Natl. Acad. Sci. U. S. A.*, 2004, **101**, 15275.
42 P. Yin, H. M. Choi, C. R. Calvert and N. A. Pierce, *Nature*, 2008, **451**, 318.
43 B. L. Li, A. D. Ellington and X. Chen, *Nucleic Acids Res.*, 2011, **39**, e110.
44 Z. Cheglakov, T. M. Cronin, C. He and Y. Weizmann, *J. Am. Chem. Soc.*, 2015, **137**, 6116.
45 H. M. Choi, J. Y. Chang, L. A. Trinh, J. E. Padilla, S. E. Fraser and N. A. Pierce, *Nat. Biotechnol.*, 2010, **28**, 1208.
46 D. P. Bartel, *Cell*, 2004, **116**, 281.
47 J. T. Pena, C. Sohn-Lee, S. H. Rouhanifard, J. Ludwig, M. Hafner, A. Mihailovic, C. Lim, D. Holoch, P. Berninger, M. Zavolan and T. Tuschl, *Nat. Methods*, 2009, **6**, 139.
48 G. Obernosterer, J. Martinez and M. Alenius, *Nat. Protoc.*, 2007, **2**, 1508.
49 J. Ge, L. Zhang, S. Liu, R. Yu and X. Chu, *Anal. Chem.*, 2014, **86**, 1808.
50 R. Deng, L. Tang, Q. Tian, Y. Wang, L. Lin and J. Li, *Angew. Chem., Int. Ed.*, 2014, **53**, 2389.
51 F. Porichis, M. G. Hart, M. Griesbeck, H. L. Everett, M. Hassan, A. E. Baxter, M. Lindqvist, S. M. Miller, D. Z. Soghoian, D. G. Kavanagh, S. Reynolds, B. Norris, S. K. Mordecai, Q. Nguyen, C. Lai and D. E. Kaufmann, *Nat. Commun.*, 2014, **5**, 5641.
52 D. Koley and A. J. Bard, *Proc. Natl. Acad. Sci. U. S. A.*, 2010, **107**, 16783.
53 Z. Zhang, Z. Zhu, K. Watabe, X. Zhang, C. Bai, M. Xu, F. Wu and Y. Y. Mo, *Cell Death Differ.*, 2013, **20**, 1558.
54 S. M. Zhu, H. L. Wu, F. T. Wu, D. T. Nie, S. J. Sheng and Y. Y. Mo, *Cell Res.*, 2008, **18**, 350.
55 B. N. Hannafon, K. J. Carpenter, W. L. Berry, R. Janknecht, W. C. Dooley and W. Q. Ding, *Mol. Cancer*, 2015, **14**, 133.

